Author's personal copy

Ultrasound in Med. & Biol., Vol. 40, No. 1, pp. 232–243, 2014
Copyright © 2014 World Federation for Ultrasound in Medicine & Biology
Printed in the USA. All rights reserved
0301-5629/$ - see front matter

http://dx.doi.org/10.1016/j.ultrasmedbio.2013.08.010

● *Original Contribution*

A 3-D ULTRASOUND IMAGING ROBOTIC SYSTEM TO DETECT AND QUANTIFY LOWER LIMB ARTERIAL STENOSES: *IN VIVO* FEASIBILITY

Marie-Ange Janvier,*† Samir Merouche,*† Louise Allard,* Gilles Soulez,†‡§ and Guy Cloutier*†§

*Laboratory of Biorheology and Medical Ultrasonics, Research Center of the University of Montreal Hospital (CRCHUM), Montréal, Québec, Canada; †Institute of Biomedical Engineering, University of Montreal, Montréal, Québec, Canada; ‡Department of Radiology, University of Montreal Hospital (CHUM), Montréal, Québec, Canada; and §Department of Radiology, Radio-Oncology and Nuclear Medicine, University of Montreal, Montréal, Québec, Canada

(*Received* 30 *November* 2012; *revised* 8 *August* 2013; *in final form* 12 *August* 2013)

Abstract—The degree of stenosis is the most common criterion used to assess the severity of lower limb peripheral arterial disease. Two-dimensional ultrasound (US) imaging is the first-line diagnostic method for investigating lesions, but it cannot render a 3-D map of the entire lower limb vascular tree required for therapy planning. We propose a prototype 3-D US imaging robotic system that can potentially reconstruct arteries from the iliac in the lower abdomen down to the popliteal behind the knee. A realistic multi-modal vascular phantom was first conceptualized to evaluate the system's performance. Geometric accuracies were assessed in surface reconstruction and cross-sectional area in comparison to computed tomography angiography (CTA). A mean surface map error of 0.55 mm was recorded for 3-D US vessel representations, and cross-sectional lumen areas were congruent with CTA geometry. In the phantom study, stenotic lesions were properly localized and severe stenoses up to 98.3% were evaluated with –3.6 to 11.8% errors. The feasibility of the *in vivo* system in reconstructing the normal femoral artery segment of a volunteer and detecting stenoses on a femoral segment of a patient was also investigated and compared with that of CTA. Together, these results encourage future developments to increase the robot's potential to adequately represent lower limb vessels and clinically evaluate stenotic lesions for therapy planning and recurrent non-invasive and non-ionizing follow-up examinations. (E-mail: guy.cloutier@umontreal.ca) **© 2014 World Federation for Ultrasound in Medicine & Biology.**

Key Words: **3-D ultrasound imaging system, 3-D reconstruction, Robotics, Vascular phantom, Lower limb arterial disease, Computerized tomography angiography, Arterial stenosis.**

INTRODUCTION

Atherosclerosis causes peripheral arterial disease through the formation of diffuse lesions in vessels of the lower limbs (Watson et al. 2006). Reduction of arterial diameter by more than 50% represents significant stenosis, possibly requiring invasive therapy (*i.e.*, endovascular or surgical revascularization) (Collins et al. 2007). Usually, these procedures require planning with precise information on stenosis severity, location, length and non-diseased vessel diameter. It is common to follow the patency of endovascular or surgical therapy to detect restenosis or progression of atherosclerosis (Landry et al. 2003). Indeed, the rate of restenosis 1 y after balloon dilation and stenting of the femoro-popliteal artery is around 40% to 60% (Schillinger et al. 2006). The patency of vein graft bypass also requires long-term surveillance because of the occurrence of stenoses through myo-intimal hyperplasia (Leotta et al. 2003).

Ultrasound (US) is the first-line imaging method employed clinically to investigate lower limb arterial lesions. Diagnosis relies on pulsed-wave Doppler and color Doppler flow assessment, as well as B-mode imaging to define atherosclerotic plaque morphology (Chan et al. 2010). Because most US-based evaluation methods are limited to 2-D image plane views, they do not provide sufficient information to guide interventional therapy. After indicated by US screening, invasive therapy for symptomatic peripheral arterial disease is planned non-invasively with computed tomography angiography (CTA) and magnetic resonance angiography scan or invasively with digital subtraction angiography

Address correspondence to: Guy Cloutier, Laboratory of Biorheology and Medical Ultrasonics, University of Montreal Hospital Research Center (CRCHUM), Pavillion J.A. de Sève (Room Y-1619), 2099 Alexandre de Sève, Montréal, Québec, Canada H2L-2W5. E-mail: guy.cloutier@umontreal.ca

Author's personal copy

(Collins et al. 2007; Chan et al. 2010). Although the latter imaging techniques can map the entire lower limb vascular tree in 3-D rendering, computed tomography (CT) imaging is ionizing and requires the injection of allergenic iodine contrast agent, whereas magnetic resonance angiography is costly. Moreover, the gadolinium-based contrast can induce nephrogenic systemic fibrosis in patients with renal failure and is limited by several contra-indications related to the high magnetic field. Given the importance of quantifying stenoses and mapping their localization for therapy planning and patient follow-up, the development of a precise non-invasive US-based 3-D mapping technique is of clinical importance for vascular evaluation of the lower limbs.

Three-dimensional US imaging is an economical and tolerable technology used mainly in research for anatomic or volume representation. Because it can provide the physician with a complete map of lower limb vessels, it has the potential to increase confidence in the diagnosis and provide accurate localization and quantification of stenoses. The use of 3-D US systems based on linear step motors, and electromagnetic and optical freehand tracking techniques, *in vivo* to image carotid arteries, lower limb venous bypasses and the brachial plexus (*i.e.*, nerve fibers running from the spine to the neck, armpit and arm) has been found to be feasible (Lee et al. 2004; Barratt et al. 2004; Cash et al. 2005; Landry et al. 2005; Leotta et al. 2005a). These devices are ideal for localizing lesions on short segments, but the restricted range of probe motion detection, signal interference or tracking visibility limits their utility in long and tortuous lower limb arteries (Birkfellner et al. 1998; Cartelieri et al. 2001; Frantz et al. 2003).

Robotic systems represent an alternative for localization and quantification of lower limb stenoses because they can simultaneously control and standardize the 3-D US image acquisition process with high precision and flexibility. Although most 3-D US prototype robots attempt to increase the capability of clinicians in prostate brachytherapy and tele-echography of the abdomen (Arbeille et al. 2003; Lagerburg et al. 2006; Bax et al. 2008), only two designs exist for vascular examination. Hippocrate is the first feedback medical robot designed with tolerability strategies to scan short vessel segments, such as the carotid artery, and to perform tonometry measurements synchronized with the heart rate (Pierrot et al. 1999). To the best of our knowledge, other than a non-invasive investigation of endothelial function (Levenson et al. 2001), no follow-up study has been conducted with this robot. In fact, the robot's mechanical architecture was later adapted to a new design for reconstructive skin surgery (Dombre et al. 2003). The University of British Columbia's medical US image-guided robot is designed for tele-examination scanning of the carotid artery (Abolmaesumi et al. 2002). Shared control between operators, the robot controller and US image processor make the real-time visual servoing of US probe movements possible. Nevertheless, this robot's architectural design has constrained movements in its workspace and a limited 3 degrees of freedom controller because it is designed to cover the short, straight path of the carotid artery.

To provide accurate 3-D US scanning of lower limb vessels, a 3-D US imaging robotic system was developed by our group (Janvier et al. 2008). The system can scan short and long segments of leg arteries in "freehand," using a "teach" mode, and reproduce the manually taught path in "replay" mode. When scanning along a path with this robot, clinicians can acquire 2-D axial US images with their corresponding x, y and z positions at a constant speed and contact pressure to correctly represent vessels in three dimensions. The robust positioning accuracy and repeatability achieved previously over the robot's entire workspace disclosed the broad operational range of our system for eventually tracking lower limb vessels (Janvier et al. 2008). Also, we recently illustrated, with a Z-fiducial calibration procedure, that we could adequately register 2-D US images into our robot referential to reproduce a mimicked axisymmetric vessel artery with fidelity (Janvier et al. 2010). Our aim in the study described here was to determine the performance efficacy of this robotic system under conditions closer to the clinical context. Two objectives were targeted: (i) assessment of the accuracy of the robotic imaging system in locating and quantifying lower limb vessel stenoses with a phantom mimicking a realistic geometry; and (ii) evaluation of the ability of this robotic imaging system for 3-D mapping of a normal femoral artery and a diseased femoral artery *in vivo*. For both objectives, 3-D US reconstructions were compared with CTA scans in the case of diseased segments, as a gold standard examination.

METHODS

3-D ultrasound imaging robotic system

As illustrated in Figure 1, the 3-D US imaging robotic system contains a robotic arm (F3 Articulated Robot, CRS Robotics, Burlington, ON, Canada), an US echograph and a personal computer with the US robotic scanner software (Integral Technologies, Laval, QC, Canada). A Vivid-5 scanner (General Electric, Chicago, IL, USA) equipped with a FLA-10 (10 MHz) linear array probe was used for the phantom study, whereas a HDI-5000 (Philips Healthcare, Andover, MA, USA) with a L12-5 (12 MHz) linear array probe allowed *in vivo* scanning. Digitized 480 × 640-pixel format B-mode and color Doppler flow images were acquired with corresponding robotic arm positions stored for future 3-D

Author's personal copy

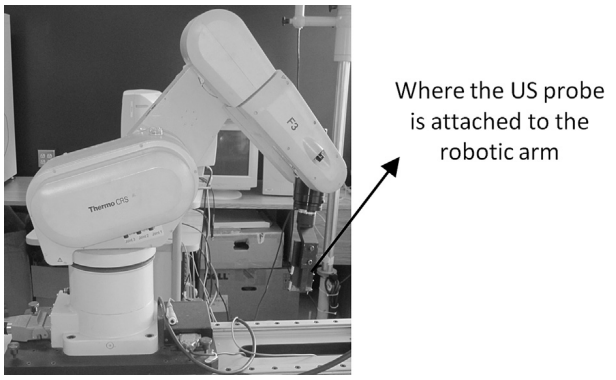

Fig. 1. F3 CRS robotic arm used in the 3-D ultrasound (US) imaging robotic system.

reconstructions. This robotic system has been described in detail (Janvier et al. 2008, 2010).

Analysis of a realistic vessel segment

Vascular phantom and experimental setup. The geometric accuracy of the robotic system in reconstructing 3-D vessels was evaluated with a phantom replicating a human iliac artery with multiple stenoses. This model was created from a 3-D reformation of a multi-detector CT scan acquisition in a patient with a peripheral arterial disease of the iliac artery. The phantom was prepared according to a manufacturing process described previously (Allard et al. 2009). Figure 2 is a 3-D vessel representation obtained from the computer-aided design (CAD) file employed to prepare the molding prototype. This segment presents two severe stenoses identified as S1 and S2 with 97.3% and 98.3% area reductions, respectively. The vessel's central axis at both ends was positioned 3.4 cm from the top cover of the phantom box; it was at 4.0 cm at the location identified on the figure (Fig. 2b), and the length, *L*, of the scanned iliac segment was 98.7 mm from the aortic bifurcation.

Dimensions of CAD 3-D representations of the vessel were measured on cross-sectional planes. The maximal diameter of the non-diseased vessel segment was $D = 6.5$ mm, and the minimum diameters at stenoses were S1 = 1.4 mm and S2 = 1.2 mm (Fig. 2a). Lengths of stenoses were measured as the distance between pre-stenotic and post-stenotic maximum vessel diameters (L1 = 14.0 mm and L2 = 28.1 mm). The distance between maximum diameter reductions at both stenoses S1 and S2 was LS = 20.0 mm.

3-D US vessel representation. As performed by Janvier et al. (2010), a Z-phantom calibration procedure of the 3-D US imaging robotic system was first required to ensure correct vessel representation. This procedure estimates the calibration transform that registers the US image plane into the robot referential. Then, the vascular

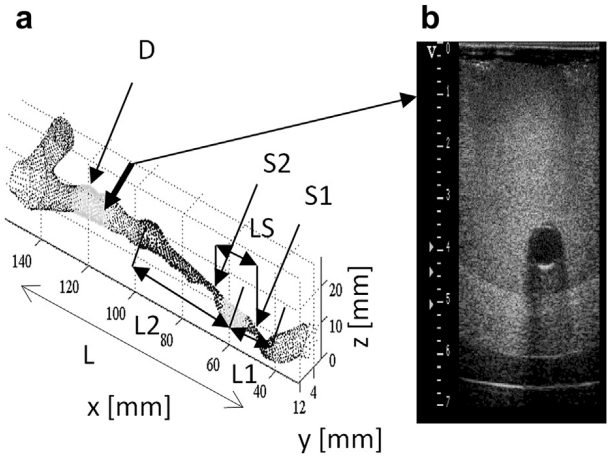

Fig. 2. (a) Computer-aided design representation of a realistic vascular phantom embodying an iliac artery with two severe stenoses (S1 and S2). L1 and L2 represent their respective lengths, and LS, the shortest distance between maximal points of the stenoses. *L* is the total length of the vessel, and *D* is the diameter of the non-diseased vessel. (b) B-mode cross-sectional image of the vascular phantom; its location is indicated by an *arrow* in (a). The shadowing on the B-mode image is attributed to the presence of a polyurethane membrane mimicking the vessel wall and used to avoid the diffusion of computed tomography angiography contrast outside the vessel lumen.

phantom filled with degassed water was set firmly into the robot's workspace. US gel was applied on the phantom's top cover, and US images were acquired at a 7-cm image depth, a 4- to 5-cm single-focus beam depth and a 3-cm window size zooming (3:7 setting on the Vivid-5 scanner) to match scanning conditions producing the best accuracy for 3-D vessel representation (Janvier et al. 2010). Then, a quasi-parallel plane US scan path was taught to the robot by a technician and automatically replayed eight times. During the robot "replay" mode, cross-sectional US images of the mimicked diseased artery were captured to reconstruct eight 3-D representations of the vessel with surface rendering. For 3-D reconstruction, the vessel lumen of each US image was segmented with a fast-marching method based on gray-level statistics and gradients adapted from Roy Cardinal et al. (2006). Then, each pixel of the segmented lumen contour was mapped into the robot referential using the calibration transform and corresponding x, y, z probe positions (Janvier et al. 2010). To provide a 3-D surface rendering of the reconstructed vessel, the transformed lumen contours were resampled on a 300 × 20 rectangular grid, interpolated and realigned normal to the vessel center axis, as performed by Leotta et al. (2001).

Computed tomography angiography representation of the vessel. Because CTA imaging has the best accuracy for peripheral arterial disease evaluation (Chan et al. 2010), a Somatom Sensation 64-slice scanner (Siemens,

Author's personal copy

Erlangen, Germany) was used to acquire images of the vascular phantom according to a standard clinical protocol. The imaging settings were: 217-mA current density, 120-kV peak voltage, 1.0-mm slice thickness, 0.6-mm reconstruction interval and 38.0-cm field of view for a 512 × 512 matrix size. The phantom lumen was filled with a 2.8% v/v (volume concentration) solution of 430 mg/mL iothalamate meglumine (Conray 43, Mallinckrodt Medical, Pointe-Claire, QC, Canada) diluted in 0.9% NaCl solution. 3-D CTA image representation was achieved with a maximum intensity projection, a volume rendering reformation and 2.0-mm axial reformations, with Visual software (Version 1.4, Object Research System, Montreal, QC, Canada). This representation was later transformed into a 3-D binary file that was converted into 3-D contour points with MATLAB (Version 6.5, The MathWorks, Natick, MA, USA).

Geometric evaluation of 3-D vessel representations. The reconstructed lumen surface, vessel cross-sectional areas, and localization and quantification of stenoses imaged with the 3-D US robotic system were compared with those obtained with the CTA gold standard method. Given that each imaging approach presents its own sources of errors, accuracy in 3-D vessel representation was also determined with the CAD file used to produce the vascular phantom.

Comparative analyses of the reconstructed surfaces. Before comparing vessel geometries, a rigid registration was performed by using an iterative closest point algorithm to align the two 3-D vessel models (Besl and McKay 1992). This method, applied on free-form curves, surfaces and 3-D shapes, efficiently matches two ranges of data points without requiring pre-processing or feature extraction. The algorithm uses a closest point estimation method and an iterative absolute orientation algorithm (Horn 1987). The result is an optimal transformation matrix (translation and rotation) that minimizes the mean square distance between the two 3-D models.

Surface reconstruction errors were evaluated by measuring the absolute distance between points on the 3-D evaluated geometry and on the gold standard vessel representation, as expressed by

$$E_{i,j,k} = S_{\text{tested}}(i,j,k) - S_{\text{ref}}(i,j,k) \quad (1)$$

where S_{tested} is the surface points of the 3-D reconstructed vessel evaluated; S_{ref} is the surface points of the reference method; $1 \leq i \leq X$, where X is the number of grid points along the x-axis; $1 \leq j \leq Y$, where Y is the number of points along the y-axis; and $1 \leq k \leq Z$, where Z is the number of points along the z-axis. If the number of cross sections differs between US, CTA and CAD 3-D models, eqn (1) uses for reference the representation with the minimum longitudinal distance X. For all comparisons of 3-D reconstructions between US (B-mode, color flow), CTA and CAD files, the absolute value of this measure was tabulated into one mean (sample size = $X \times Y \times Z$, where chosen dimensions were those of the reference model).

Lumen cross-sectional areas. Cross-sectional areas were measured along the x-axis of each 3-D reconstructed vessel on US (B-mode and color flow) and CTA and on the CAD file. The area was evaluated with *Polyarea,* a polygon-specific function of MATLAB, which computes the average number of pixels inside a clockwise closed contour. For all eight US reconstructions, the mean (±standard deviation) cross-sectional areas were assessed over the vessel length (sample size = X, which is the number of cross sections).

Localization and quantification of stenoses. Stenoses were localized at perceived stenotic sites. Stenoses were quantified as the percentage of lumen reduction compared with a reference vessel in surface. This measure, S_{area}, is expressed as

$$S_{\text{area}} = 100 \times \left(\frac{A_D - A_i}{A_D} \right) \quad (2)$$

where A_i defines the area of a cross-sectional vessel lumen, and A_D expresses the reference measure where the maximal value is identified in the non-diseased vessel segment (see label *D* in Fig. 2). S_{area} was evaluated with respect to the known degree of vessel narrowing, as determined by the CAD file of the 3-D vessel representation (see *S* labels in Fig. 2). The degree of stenosis was the maximal quantified value at the stenotic site. Dimensions of stenoses were measured in terms of length using the CAD file 3-D representation of the vessel for reference (labels *L1, L2* and *LS* in Fig. 2).

In vivo feasibility study

3-D US imaging robotic system: Experimental setup, data acquisition and processing. To evaluate the feasibility of the robotic system, a pilot study was first realized on a normal volunteer and then conducted on a patient, an 82-y-old man with evidence of occlusive peripheral arterial disease, as indicated by a previous CTA exam. The study received approval from our institutional review board and informed consents were obtained.

The volunteer lay supine with the target limb rose to the height of a supportive pillow. The radiologist first manipulated the US probe attached to the robotic arm in "teach mode" (*i.e.*, a mode enabling the learning of a "freehand" scan with minimum torque applied on robot

Author's personal copy

articulations) to inspect the femoral artery, starting from the femoral bifurcation and progressing to the distal femoral artery. The normal volunteer underwent a B-mode scan, whereas the patient underwent both B-mode and color Doppler flow exams, in teach mode, to store the femoral artery's path. These taught trajectories were then replayed by the robot at a constant speed with x, y, z coordinate registration for each acquired cross-sectional image.

Ultrasound image settings in both B-mode and color flow mode were an image depth of 6 cm, a 2- to 4-cm focus beam depth and no zooming. In B-mode, the scan path was close to perpendicular with respect to the longitudinal axis of the vessel. In color flow mode (patient), optimal angles allowing Doppler shift to fill the vessel lumen, according to the perception of the clinician, were chosen along the scan path (the mean angle was determined in post-processing from the x, y, z coordinates of each acquired image and was 54.4°). The wall filter was set to 87 Hz. The subject's leg remained seemingly immobile throughout the entire examination, but movements were not monitored. Collected images were then analyzed and processed for 3-D vessel reconstructions according to the same methods described for the phantom study.

Computed tomography angiography experimental setup, data acquisition and processing. The lower limb CTA examination of the patient was performed with the same scanner and aforementioned parameter settings as in the phantom study. The patient was placed in a supine position, feet first in the scanner with legs at the isocenter, and a sweep was executed from the abdominal aorta to the patient's foot with a 40.0-cm field of view. A 120-cc bolus of the non-ionic contrast agent Omnipaque 370 (iohexol 370 mg iodine/mL, GE Healthcare, Buckinghamshire, UK) was injected at the rate of 4 cc/s with an intravenous superficial brachial catheter. Collected data were processed to reconstruct in three dimensions the right femoral artery. No volume rendering was performed. Calcifications in CT scans were excluded from the vessel lumen based on threshold methods. The reformation was created from the lumen outline.

Geometric comparison of 3-D vessel representations. For the patient, geometric analyses of the lower limb femoral artery reconstructed from US and CTA images were conducted by aligning the corresponding segment from the femoral bifurcation. The reconstructed surface and lumen cross-sectional areas were then compared; stenosis were also quantified. All methods for 3-D rigid registration and performance assessment metrics were described earlier under Vascular Phantom and Experimental Setup.

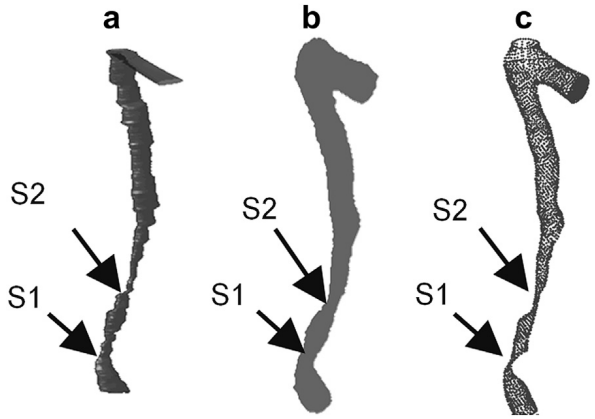

Fig. 3. Three-dimensional vessel representations of the realistic vascular phantom with two severe stenoses (S1 and S2) illustrated by (a) 3-D US (B-mode), (b) computed tomography angiography and (c) the computer-aided design file.

RESULTS

Analysis of a realistic vessel segment mimicking an iliac diseased artery

Comparative analyses of 3-D vessel representations. In Figure 3 are examples of the vascular phantom lumen imaged with the 3-D US system in B-mode and the computed tomography angiography (CTA) scanner, as well as the corresponding gold standard CAD file. Table 1 tabulates the total artery length and surface area of these three vessel maps. Three-dimensional US provided the shortest vessel representation and the smallest surface, whereas CTA had the largest surface area compared with the CAD file. In Figure 4 are comparative surface error maps for CTA and 3-D B-mode US comparisons, CAD versus 3-D US and CAD versus CTA. For 3-D B-mode US assessment, eight reconstructions were used for comparisons, and results were tabulated into one mean to display a surface error map.

In the displays of Figure 4, surface contour points were compared with the closest surface contour points of the reference model. Because the number of cross-sections differs between US, CTA and CAD 3-D maps, in eqn (1), the representation with the minimum longitudinal distance X was used for reference. Thus, overestimations with respect to the reference 3-D maps (B-mode in Fig. 4a and CAD in Fig. 4b and c) are shown in green-yellow to red, whereas underestimations are displayed in navy blue to dark blue. Therefore, in the evaluation performed between each representation, missing lengths (i.e., missing cross-sections) at the extremity resulted in large errors because the closest reference surface points used in eqn (1) were enlarged; we kept this information, but it should not be viewed as an image reconstruction distortion.

Author's personal copy

Table 1. Comparative analysis of 3-D reconstructed surfaces of the realistic vascular phantom

3-D vessel representation	Total length L (mm)	Total surface (mm^2)	Number of samples
3-D ultrasound (B-mode)	89.4 ± 0.7	1884.5 ± 7.1	8
CTA	95.9	2073.2	1
CAD	98.7	2015.9	1

CAD = computer-aided design; CTA = computed tomography angiography.

As seen in Figure 4a, CTA (tested geometry) in eqn (1) provided an overestimated vessel representation of the reconstructed surface compared with 3-D US (referenced geometry). The absolute mean error of eight vessel samples was 0.55 ± 0.04 mm (range: 0.03–3.6 mm) (these statistics exclude artifacts at the extremity). For each error map where the CAD file was the gold standard reference (Fig. 4b, c), the surface reconstruction error of the tested geometry generally indicates an overestimation of vessel size, except for B-mode US around the S2 stenotic site and the non-diseased area for CTA, where an underestimation is noted. Three-dimensional US (B-mode) had an absolute mean surface error of 0.96 ± 0.54 mm (range: 0.06–3.6 mm) (Fig. 4b). CTA disclosed the smallest errors of 0.60 ± 0.39 mm (range: 0.05–2.2 mm) (Fig. 4c).

Figure 5a is an example, from one B-mode US reconstruction, of the cross-sectional lumen x, y, z orientation along the vessel axis, whereas Figure 5b compares quantitatively areas obtained in B-mode US (n = 8), CTA and CAD. CTA gave the largest representation of the vessel lumen compared with the CAD file, with a mean cross-sectional area error of 10.7 ± 11.3 mm^2 along x, whereas 3-D B-mode US resulted in a smaller mean cross-sectional area error of 4.3 ± 12.6 mm^2. The 3-D US vessel cross-sectional areas compared with CTA had a mean error of –6.4 ± 9.8 mm^2.

Localization and quantification of stenoses. Stenoses S1 and S2 were localized in each 3-D vessel representation (Fig. 5). They were then quantified according to eqn (2) and summarized in Table 2. Both stenoses, in area reduction, were better assessed in 3-D B-mode US than with CTA. Table 3 summarizes lengths of stenoses; errors were either larger than, equivalent to or smaller than those for 3-D US than CTA, compared with the CAD file.

In vivo feasibility study

Figure 6 provides the 3-D US B-mode reconstruction of the normal superficial femoral artery of the volunteer. The color map expresses the area in square millimeters. Figure 7 is a volume rendering reformation

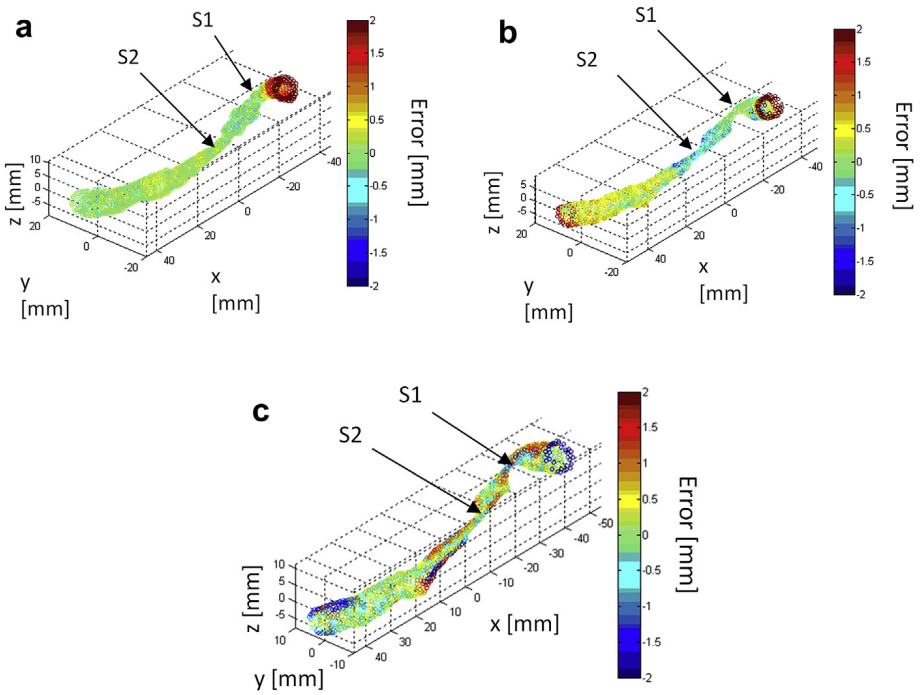

Fig. 4. Comparative analysis between 3-D vessel representations of the realistic vascular phantom with two severe stenoses (S1 and S2). (a) On the B-mode 3-D ultrasound (US) vessel representation, mean surface reconstruction comparison between computed tomography angiography and 3-D US is displayed. On the computer-aided design file, the respective surface reconstruction errors are shown with the (b) 3-D US (B-mode) and the (c) computed tomography angiography.

Author's personal copy

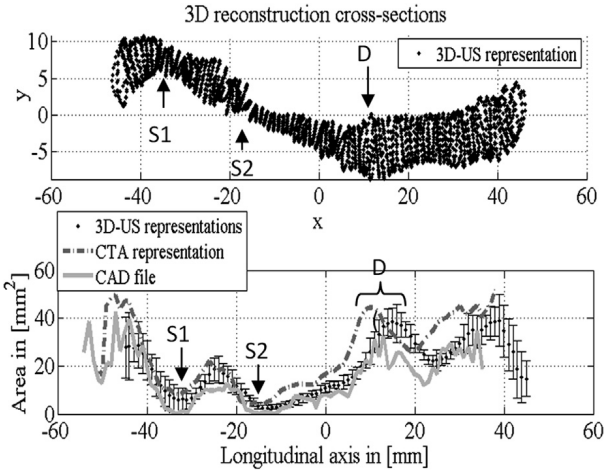

Fig. 5. Cross-sectional lumen areas of the 3-D ultrasound (US), computed tomography angiography (CTA) and computer-aided design (CAD) file representations for the realistic vascular phantom. S1 and S2 represent severe stenoses, and *D* is the diameter of the non-diseased vessel.

of the CTA acquisition of the patient's right common and superficial femoral arteries displaying calcification and multiple stenoses. Figure 8a provides the CTA vessel representation with zooming of the middle segment (Fig. 8b and d) to show comparisons of surface maps with 3-D B-mode US and 3-D color Doppler US. Corresponding error maps are presented in Figure 8(c, e), and quantitative assessments of the middle segment total length and surface area in each mode are summarized in Table 4. The B-mode 3-D vessel representation provided a larger surface and length, and Doppler, shorter ones. As reported in Figure 8(c, e), both 3-D US vessel representations overestimated the CTA middle segment reconstructed surface points. The absolute mean surface reconstruction error using eqn (1) of the B-mode 3-D vessel representation compared with CTA was 1.82 ± 1.31 mm (range: 0.02–6.1 mm) (Fig. 8c). It was doubled for color Doppler; indeed, the absolute mean error was 2.99 ± 2.10 mm, and the range, 0.03–9.31 mm (Fig. 8e). Note that both statistics exclude artefacts at the extremity. Similar conclusions can be made regarding the cross-sectional lumen areas evaluated in the middle vessel section in Figure 9. Two moderate stenoses of 49.9% and 56.3% were quantified in the CTA longitudinal segment of [–60, –40] and [–20, 20] mm (see Fig. 9). In Doppler, the corresponding stenoses were localized at [–40, –20] and [0, 20] mm and quantified to 71.3% and 78.6%, respectively. In B-mode, stenoses were localized at [–40, 0] and [0, 20] mm with quantifications of 88.9% and 89.8%.

Table 2. Quantification of stenoses of the realistic vascular phantom

		B-mode ultrasound (8 samples)		CTA (1 sample)	
CAD	Stenosis (%)	Measurement	Error	Measurement	Error
S1	97.3	85.6 ± 6.1	–11.8 ± 6.1	81.5	–15.8
S2	98.3	94.8 ± 1.9	–3.6 ± 1.9	91.5	–6.9

CAD = computer-aided design; CTA = computed tomography angiography.

Table 3. Lengths of stenoses of the realistic vascular phantom

		B-mode ultrasound (8 samples)		CTA (1 sample)	
CAD	Length (mm)	Measurement	Error	Measurement	Error
L1	14.0	14.4 ± 2.5	0.4 ± 2.5	12.0	–1.96
L2	28.1	31.6 ± 2.0	3.5 ± 2.0	29.1	1.0
LS	20.0	19.0 ± 2.6	–1.1 ± 2.5	28.1	–8.1

CAD = computer-aided design; CTA = computed tomography angiography.

DISCUSSION

Analyses of 3-D vessel representations

In this study, phantom and *in vivo* 3-D US vessel representations exhibited geometries similar to those obtained with the clinical CTA gold standard. The phantom investigation revealed that 3-D US reconstructed surfaces had a mean difference from CTA of less than 1 mm (0.55 mm); *in vivo,* a larger mean difference of 1.82 mm was noted. Larger errors noted at the extremities exist because of differences in length between 3-D representations. Although comparable B-mode (or color Doppler) versus CTA results were obtained, the reliability of computed tomography can be discussed because the true gold standard CAD file was available for the phantom study. CTA overestimated true vessel size (surface area of 2073 mm^2 vs. 2016 mm^2 for CAD [Table 1]; also see Fig. 5b). This can be explained by the maximum intensity projection and volume rendering algorithms used to outline the lumen boundary of CTA images and by the smooth filtering applied along the longitudinal axis. With these algorithms, there can be significant loss of detail in CTA scans because only one gray threshold was used to identify the lumen vessel. Consequently, CTA post-processing techniques are user dependent (Rengier et al. 2009). In addition, the resolution of CTA for lower limb vascular applications is on the order of 1 mm (Nie et al. 2012). Because the phantom had stenoses with diameters in this range (1.2–1.4 mm), even with contrast agent, loss of detail and overestimation of the lumen surface were expected. Regarding 3-D B-mode US assessment versus CAD, our findings indicated an error of 1.13 ± 0.56 mm (range: 0.06–7.1 mm)

Author's personal copy

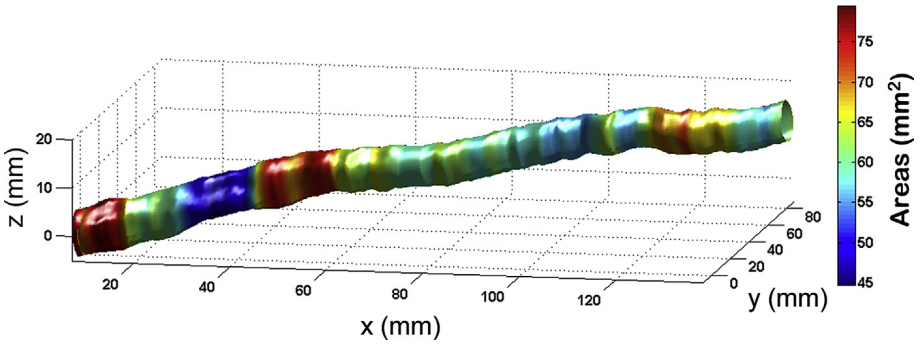

Fig. 6. Three-dimensional ultrasound vessel representation of the normal volunteer's right femoral artery mapped in area.

(Fig. 4b). Reported errors are also explained by the limited resolution of US and by the surface reconstruction procedure of the robotic system, explained further by Janvier et al. (2010).

Some factors can be identified regarding the performance of the 3-D US imaging robotic system when comparisons are made either with 3-D CTA or CAD mappings. Considerable differences are observed between B-mode and CTA representations in the phantom study (Figs. 4a and 5) and *in vivo* (Figs. 8 and 9): the B-mode representation was closer to CTA in the phantom study than *in vivo*. Although different segmentation methods were used, it is important to note that the most significant challenge faced with *in vivo* CTA images was identification of the vessel lumen from surrounding tissues and exclude vascular calcifications. For US, the fast matching segmentation method has been reported to be quite robust (Roy Cardinal et al. 2006), but errors caused by calcium shadowing cannot be excluded. Thus, errors in segmentation could have been introduced into the *in vivo* CTA and US representations. Regarding specifically 3-D US, discrepancies with CTA could also result from the number of image samples along the *x*-axis (longitudinal axis) and the 3-D calibration precision of the robotic system. Also, contrary to CTA representations that were smoothed along the longitudinal axis, 3-D US mappings were presented by juxtaposing raw *x*, *y*, *z* segmentation points of each cross-sectional image (*e.g.*, see Figs. 5a and 9a and b). Together, these errors were found, in a previous study, to contribute to up to 0.40 mm in surface point reconstruction and are thoroughly discussed in Janvier et al. (2010). Other sources of error could reside in the process of fabrication of the vascular phantom, with reported errors up to 5.7% in diameter compared with the CAD file (Allard et al. 2009). However, all above-mentioned sources of error do not explain entirely 3-D mapping discrepancies with CTA or CAD reconstructions, especially *in vivo* (Fig. 9).

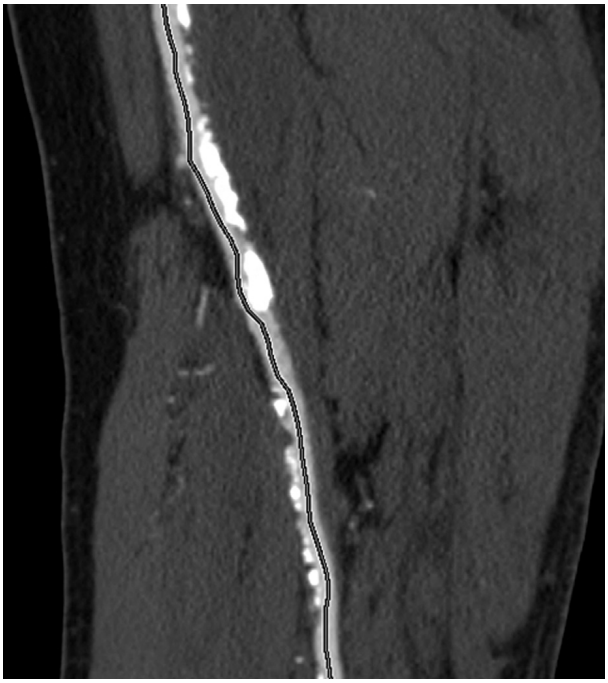

Fig. 7. Volume rendering 3-D reformation of the computed tomography angiography of the patient's right femoral artery.

The same calibration transform sources of error (*i.e.*, Z-phantom calibration) were faced in the phantom study and *in vivo*, except that the location of the calibration phantom in the robot workspace could have an effect on the 3-D vessel dimensions and geometry. In the phantom study, the position of the Z-phantom and that of the scanned vascular phantom coincided, as in Janvier et al. (2010), whereas *in vivo* the Z-phantom was located approximately within the robot workspace. Indeed, the subject's leg was first scanned, markers were indicated on the scanning bed and then the Z-phantom was positioned approximately at the location of the middle segment of the femoral artery. That explains why only the middle segment of the femoral artery was reconstructed and compared with CTA for the patient (in Fig. 8). Note, however, that for the normal volunteer in Figure 6, a quite realistic 3-D US reconstruction was

Author's personal copy

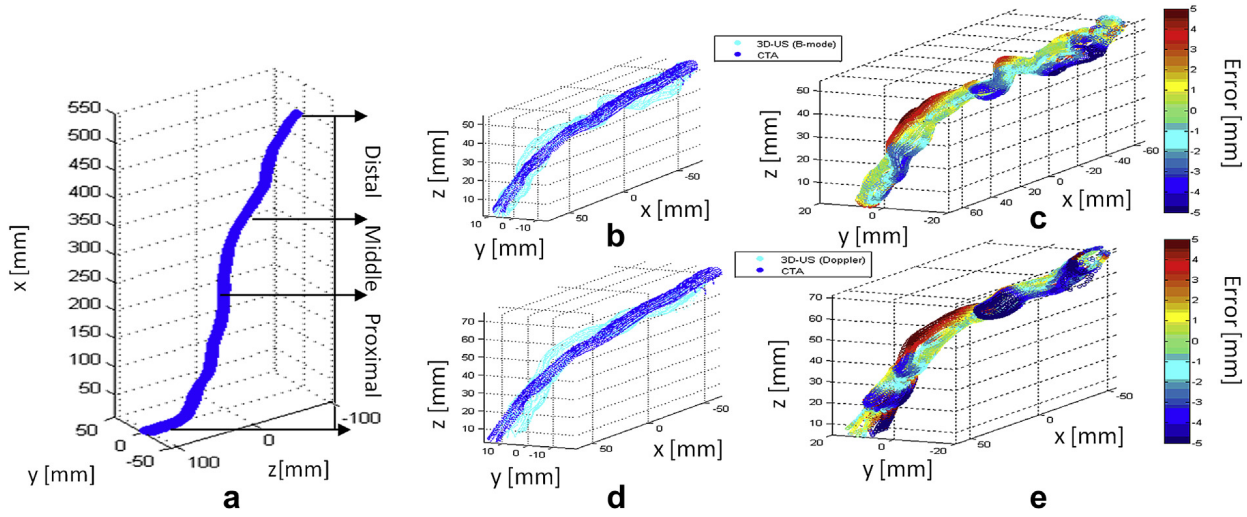

Fig. 8. (a) Entire computed tomography angiography vessel representation of the patient's right femoral artery divided into three segments: proximal, middle and distal. (b) The middle segment (from 220 to 370 mm) in B-mode. (c) Surface map errors on the 3-D ultrasound vessel representation. (d) Same middle vessel segment in color Doppler flow. (e) Surface map errors with respect to computed tomography angiography representation.

obtained. Even if reliability could not be proven because a CTA comparison could not be done, this observation leads us to postulate that the *in vivo* Z-phantom calibration was not a major source of error.

As introduced earlier, "subjects' motion" was not monitored in this study, and the current version of our robotic scanner could not compensate for that. The robot tags positions of US images and assumes the vessel to be static between the freehand teach and automated scanning modes. According to the results in Figure 6 (volunteer) and Figure 8 (patient), movements likely occurred when scanning the femoral artery of the patient. To verify this hypothesis, we re-scanned the normal subject by asking him to intentionally move his leg upward during the replay mode. The 3-D US B-mode reconstruction is presented in Figure 10. As noticed, two discontinuities are seen with a few oscillations along the artery. According to this, the discrepancy between 3-D US and CTA in Figures 8 and 9 was likely due to movement artifacts. Of course, this preliminary *in vivo* feasibility study is not enough to characterize the 3-D US imaging robotic system, but holds great promise for future clinical perspectives and repetitive non-invasive therapy follow-up.

Table 4. Comparative analysis of 3-D reconstructed surfaces of the middle segment of the patient's right femoral artery

3-D vessel representation	Total length L (mm)	Total surface (mm^2)	Sample size (N)
B-mode	136.6	2868.6	1
Doppler	115.8	2431.8	1
CTA	128.7	2702.7	1

CTA = computed tomography angiography.

Analyses of localization and quantification of stenoses

Severe phantom stenoses were detected, localized and quantified (see Fig. 5 and Table 2). Compared with CTA, B-mode incorrectly estimated the lumen areas of S1 and S2 by less than 4.1%. The difference was much larger with CAD file representations (see Table 2), where stenoses were generally under-valued by up to 11.8%. The difference in stenosis quantification was mostly due to the poor assessment of the non-diseased vessel segment, where dimensions (in area) were larger with CTA than in the CAD file and 3-D US representations

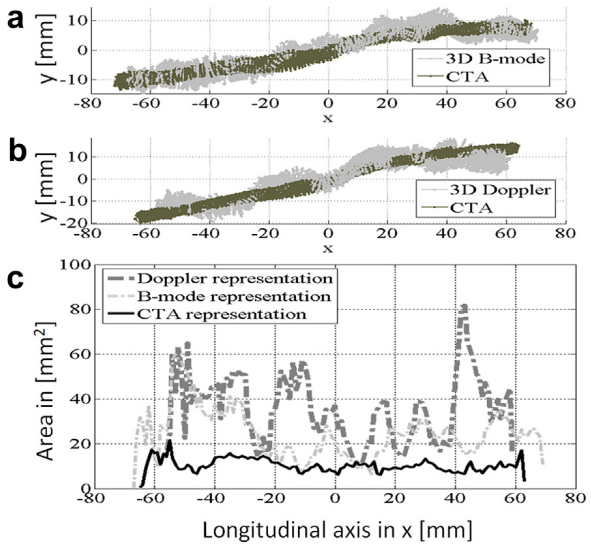

Fig. 9. (a, b) Computed tomography angiography (CTA) 3-D vessel representation of the middle segment of the patient's right femoral artery in B-mode (a) and color Doppler flow (b). (c) Corresponding cross-sectional lumen areas.

Author's personal copy

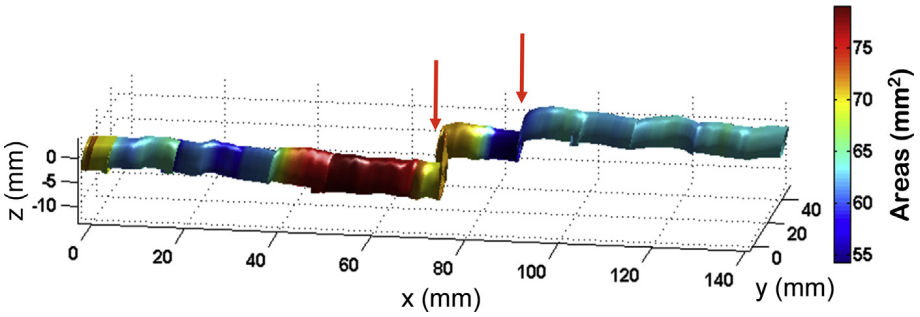

Fig. 10. Three-dimensional ultrasound vessel representation of the normal volunteer's right femoral artery mapped as lumen area in square millimeters. In this example, the subject intentionally moved upward during image acquisition to produce artifacts.

(Table 1 and Fig. 5). Also, S2 was more accurately quantified than S1 probably because in the fabrication of the vascular phantom, this segment was more congruent to the CAD file (Fig. 5). In Table 3, lengths of stenoses in 3-D US and CTA representations had errors of different magnitude with the CAD file (<8.1 mm).

In vivo, detection and quantification of stenoses on 3-D US vessel representations (both B-mode and Doppler) were more difficult because vessel axes did not perfectly overlap with CTA (Fig. 8). Note that severe stenoses were not easily identifiable as well on the CTA representation. Moderate *in vivo* stenoses were quantified on 3-D US vessel representations up to 89.8% in B-mode and up to 78.6% in Doppler (see Fig. 9 zones [–40, 0] and [0, 20] mm); the CTA was quantified up to 39.0% (see Fig. 9 zones [–60, –40] and [–20, 20] mm). This was mostly attributed to differences in the geometry of the non-diseased segment on 3-D US vessel representations. Because the true vessel area is unknown *in vivo* and because only one patient was used, it is premature to make conclusions on the capability of the robotic scanning system to quantify stenoses in patients.

Comparison with the literature

Analyses of 3-D vessel representations. Reconstruction of a realistic vessel segment (89.4 mm in length) was achieved reliably in the phantom study with the 3-D US robotic imaging system, as compared with CTA. A mean surface-reconstructed error of 0.55 mm, which translates across its length as 0.65% variability (percentage of surface-reconstructed error/length) was reported, and a mean lumen cross-sectional error of –6.4 ± 9.8 mm^2 with respect to CTA was found. *In vivo*, the middle segment of a lower limb artery imaged in CTA was reconstructed with US (136.6 mm in length). This portion was biased, with a mean point surface error of 1.82 mm in B-mode that translates across its length into a 1.34% variability (percentage of surface-reconstructed error/length) and a mean lumen cross-sectional area error of 13.4 ± 11.1 mm^2. The same analyses were doubled in value for the color Doppler representation. In the literature, it is difficult to compare our results with other 3-D US studies using electromagnetic freehand tracking because they have not evaluated the accuracy of their systems and have focused mainly on demonstrating their technology's potential to monitor pathologic changes in reconstructed vessels during a fixed period. For example, in a carotid study, four asymptomatic patients with almost non-existent atherosclerosis plaque were used to evaluate the reproducibility of a freehand system to assess vessel lumen volume (Allott et al. 1999). The carotid artery lumen volume had 5% (cm^3) reproducibility, but only a 1-cm segment of its bifurcation was analyzed. In a vein graft investigation (Leotta et al. 2003), the cross-sectional lumen area was monitored at affected sites (*e.g.*, valves and diffused intimal hyperplasia), and the reproducibility of the electromagnetic tracking system in 10 patients was 6.9% (2.5 mm^2) for lengths ranging from 16 to 75 mm. Other studies examining the carotid artery evaluated the reproducibility to 1.4% root mean square precision with phantoms that consisted of water-filled balloons, and illustrated the reconstruction of two *in vivo* pathologic geometries without performing any analyses (Barry et al. 1997). Another study validated their reproducibility with anthropomorphic pulsatile phantoms of the carotid bifurcation of approximately 40 mm in length (Barratt et al. 2004). Errors in cross-sectional areas were up to –6.5% (–1.5 mm^2), and their lumen volume, up to –5.5% (–89.9 mm^3). The applicability of this system was tested *in vivo* on four pathologic patients with no image reference for analyses.

All these methods seem promising to reproduce results with high fidelity in vessel segments. Our data also have comparable reproducibility for vessel reconstruction in a phantom study and *in vivo* across its length. However, we have also illustrated the accuracy of vessel representations in a phantom and compared our *in vivo* results with a reference model produced by another clinical imaging modality. As we have reported, solely assessing reproducibility does not verify accuracy in

Author's personal copy

reconstructing the entire vessel geometry. This measure just indicates the stability of the system in reproducing the same 3-D representation. This sort of assessment is usually biased because the environment is controlled and does not represent the clinical context. In our study, we indicated the potential to accurately represent lower limb arteries in a phantom study with realistic vessel geometry by surface reconstruction analyses and cross-sectional area measurements. We investigated these geometries with CTA, a clinical diagnosis tool with the highest standard of accuracy, and assessed errors with the CAD file representing the geometry of the lumen. The feasibility of producing a 3-D vessel representation of a lower limb superficial femoral artery with or without stenoses *in vivo* was also tested by emulating, at best, the clinical context. The 3-D US imaging robotic system used to detect, localize and quantify lower limb arterial stenoses was presented in full scope in a manner that identifies clinical benefits and pitfalls, and further developments required to enhance the clinical application.

Analyses of localization and quantification of stenoses. Stenoses in this study were detected and quantified in terms of area reduction and length. In the phantom study, stenoses up to 98.3% (corresponding approximately to 82% in diameter) were detected with errors <4.1% with respect to CTA (<11.8% error compared with the CAD file). In the literature, only a few phantom studies performed with an electromagnetic tracking device had similar objectives. We previously tested the ability of such devices to quantify in-stent restenoses in a phantom study with maximum errors of 6.2% in area reduction (Lécart et al. 2009). In a saphenous vein bypass graft study, stenoses up to 58.0% in diameter reduction were detected with less than –1.4-mm accuracy (Hodges et al. 1994). Using a similar tracking device, another phantom study assessed stenoses up to 70% in diameter reduction at the bifurcation site of the carotid artery with <3.0% error; *in vivo* stenoses up to 74% in diameter reduction were also detected with no gold standard reference (Barratt et al. 2004). This method quite accurate *in vitro* was restricted to this small arterial segment; however, because no other clinical imaging modality was used to verify the *in vivo* results, only the potential of the technology can be claimed.

Because there is no true reference standard for vessels *in vivo*, clinical investigations are often conducted in multi-modal comparison. In our work, we evaluated phantom and *in vivo* data with CTA. This clinical diagnosis tool is known to accurately detect the presence of stenoses in more than 90% of small and moderate-sized arteries, but sometimes overestimates the degree of stenosis in heavily calcified arteries (Chan et al. 2010). Our 3-D US system had difficulty detecting and localizing severe stenoses in the middle segment of the patient's femoral artery because the geometry was distorted and data were missing. Still, improvements in stenosis quantification may be achieved *in vivo* by using image compounding, because acquiring different US views may improve the signal-to-noise ratio of images. But, as discussed, the most important improvement should be targeted toward movement compensation or development of a robotic scanning strategy that would not necessitate a teach mode. A better force feedback controller (Armendariz et al. 2012) should be envisaged to monitor the pressure applied by the probe on the lower limb. Coupling this strategy with an automatic scanning mode capable of tracking the vessel and adjusting the position of the probe with respect to the new location of the artery, if the patient moves, could be considered.

Other limitations of the robotic arm also include its inflexibility in covering certain areas of the patient's lower limb for the acquisition of cross-sectional US images. It would currently not be possible with one full scan to cover the entire vascular tree from the iliac to the tibial vessels without constraints from the robot's safety controls and architecture (Janvier et al. 2008). To improve the patient's lower limb workspace and to comply with safety issues, it would be necessary to improve the robot's kinematic design. A new medical robot architecture, specially designed for this application with strong compliance with safety concerns, is in development by our group (Lessard et al. 2007).

Future work

In the future, comparative analyses could adopt multiple imaging modalities, including duplex US (*i.e.*, anatomy and blood flow), to situate the accuracy level of the 3-D US robotic imaging system for quantifying stenoses with optional spatially registered Doppler spectral waveforms (Leotta et al. 2005b). In addition, a clinical study with more patients could validate application in the medical context by observing lower limb vessel pathology over a fixed period, evaluating therapy and monitoring plaque progression.

CONCLUSIONS

The 3-D US imaging robotic system was validated with a realistic vascular phantom. The 3-D US reconstructions obtained were analyzed for geometry and quantification of stenoses. Mean surface reconstructions were compared with CTA, and the degree of stenosis was compared with the CAD file of the phantom lumen geometry. Stenotic lesions were properly localized, and severe stenoses up to 98.3% were evaluated with –3.6 to 11.8% errors. We also verified the feasibility of this system *in vivo* in a normal volunteer and compared the

Author's personal copy

3-D reconstruction with CTA imaging in the case of a stenosed artery of a patient.

Acknowledgments—This work was supported in part by the Canadian Institutes of Health Research under Grant MOP 53244. Dr. Soulez is the recipient of a National Scientist award of the Fonds de la Recherche en Santé du Québec. Ms. Janvier was the recipient of studentship awards from the Fonds de la Recherche sur la Nature et les Technologies du Québec, TD Canada Trust, the Institute of Biomedical Engineering at the Université de Montréal, the Quebec Black Medical Association and the End of Study Grant from the Faculty of Graduate and Postgraduate Studies at the Université de Montréal. The authors are grateful to Claude Kauffmann, Zhao Qin, Boris Chayer, Marianne Fenech, Marie-Hélène Roy Cardinal and François Destrempes for discussion and technical supports. The authors are also grateful to Ovid M. Da Silva for manuscript editing.

REFERENCES

Abolmaesumi P, Salcudean SE, Wen-Hong Z, Sirouspour MR, DiMaio SP. Image-guided control of a robot for medical ultrasound. IEEE Trans Rob Autom 2002;18:11–23.

Allard L, Soulez G, Chayer B, Qin Z, Cloutier G. Multimodality vascular imaging phantoms: A new material for the fabrication of pathological 3-D vessel geometries. Med Phys 2009;36:3758–3763.

Allott CP, Barry CD, Pickford R, Waterton JC. Volumetric assessment of carotid artery bifurcation using freehand-acquired, compound 3-D ultrasound. Br J Radiol 1999;72:289–292.

Arbeille P, Poisson G, Vieyres P, Ayoub J, Porcher M, Boulay JL. Echographic examination in isolated sites controlled from an expert center using a 2-D echograph guided by a teleoperated robotic arm. Ultrasound Med Biol 2003;29:993–1000.

Armendariz J, Treesatayapun C, Baltazar A. Force feedback controller based on fuzzy-rules emulated networks and Hertzian contact with ultrasound. Mech Systems Signal Process 2012;27:534–550.

Barratt DC, Ariff BB, Humphries KN, Thom SA, Hughes AD. Reconstruction and quantification of the carotid artery birfucation from 3-D ultrasound images. IEEE Trans Med Imaging 2004;23:567–583.

Barry CD, Alliott CP, John NW, Mellor PM, Arundel PA, Thomson DS, Waterton JC. Three-dimensional freehand ultrasound: Image reconstruction and volume analysis. Ultrasound Med Biol 1997;23:1209–1224.

Bax J, Cool D, Gardi L, Knight K, Smith D, Montreuil J, Sherebrin S, Romagnoli C, Fenster A. Mechanically assisted 3-D ultrasound guided prostate biopsy system. Med Phys 2008;35:5397–5410.

Besl PJ, McKay HD. A method for registration of 3-D shapes. IEEE Trans Pattern Anal Mach Intelligence 1992;14:239–256.

Birkfellner W, Watzinger F, Wanschitz F. Systematic distortions in magnetic position digitizers. Med Phys 1998;25:2242–2248.

Cartellieri M, Vorbeck F, Kremser J. Comparison of different 3-D navigation systems by a clinical user. Acta Arch Otolaryngol 2001;258:38–41.

Cash CJ, Sardesai AM, Berman LH, Herrick MJ, Treece GM, Prager RW, Gee AH. Spatial mapping of the brachial plexus using three-dimensional ultrasound. Br J Radiol 2005;78:1086–1094.

Chan D, Anderson ME, Dolmatch BL. Imaging evaluation of lower extremity infrainguinal disease: Role of the noninvasive vascular laboratory, computed tomography angiography, and magnetic resonance angiography. Tech Vasc Interv Radiol 2010;13:11–22.

Collins R, Cranny G, Burch J, Aguiar-Ibanez R, Craig D, Wright K, Berry E, Gough M, Kleijnen J, Westwood M. A systematic review of duplex ultrasound, magnetic resonance angiography and computed tomography angiography for the diagnosis and assessment of symptomatic, lower limb peripheral arterial disease. Health Technol Assess 2007;11:1–184.

Dombre E, Duchemin G, Poignet P, Pierrot F. Dermarob: A safe robot for reconstructive surgery. IEEE Trans Rob Autom 2003;19:876–884.

Frantz DD, Wiles AD, Leis SE, Kirsh SR. Accuracy assessment protocols for electromagnetic tracking systems. Phys Med Biol 2003;48:2241–2251.

Hodges TC, Detmer PR, Burns DH, Beach KW, Strandness DE Jr. Ultrasonic three-dimensional reconstruction: In vitro and in vivo volume and area measurement. Ultrasound Med Biol 1994;20:719–729.

Horn BKP. Closed-form solution of absolute orientation using unit quaternions. J Opt Soc Am 1987;4:629–642.

Janvier MA, Durand LG, Roy Cardinal MH, Renaud I, Chayer B, Bigras P, de Guise J, Soulez G, Cloutier G. Performance evaluation of a medical robotic 3 D-ultrasound imaging system. Med Image Anal 2008;12:275–290.

Janvier MA, Soulez G, Allard L, Cloutier G. Validation of 3-D reconstructions of a mimicked femoral artery with an ultrasound imaging robotic system. Med Phys 2010;37:3868–3879.

Lagerburg V, Moerland MA, van Vulpen M, Lagendijk JJW. A new robotic needle insertion method to minimise attendant prostate motion. Radiother Oncol 2006;80:73–77.

Landry GJ, Moneta GL, Taylor LM Jr, Edwards JM, Yeager RA. Comparison of procedural outcomes after lower extremity reversed vein grafting and secondary surgical revision. J Vasc Surg 2003;38:22–28.

Landry A, Spence JD, Fenster A. Quantification of carotid plaque volume measurements using 3-D ultrasound imaging. Ultrasound Med Biol 2005;31:751–762.

Lécart M, Roy Cardinal MH, Qin Z, Soulez G, Cloutier G. In vitro instent restenoses evaluated by 3-D ultrasound. Med Phys 2009;36:513–522.

Lee KW, Wood NB, Xu XY. Ultrasound image-based computer model of a common carotid artery with a plaque. Med Eng Phys 2004;26:823–840.

Leotta DF, Primozich JF, Beach KW, Bergelin RO, Strandness DE Jr. Serial measurement of cross-sectional area in peripheral vein grafts using three-dimensional ultrasound. Ultrasound Med Biol 2001;27:61–68.

Leotta DF, Primozich LF, Beach KW, Bergelin RO, Zierler RE, Strandness DE Jr. Remodeling in peripheral vein graft revisions: Serial study with three-dimensional ultrasound imaging. J Vasc Surg 2003;37:798–807.

Leotta DF, Primozich JF, Lowe CM, Karr LN, Bergelin RO, Beach KW, Zierler RE. Measurement of anastomosis geometry in lower extremity bypass grafts with 3-D ultrasound imaging. Ultrasound Med Biol 2005a;31:1305–1315.

Leotta DF, Primozich JF, Henderson SM, Karr LN, Bergelin RO, Beach KW, Zierler RE. Display of spatially-registered Doppler spectral waveforms and three-dimensional vein graft geometry. Ultrasound Med Biol 2005b;31:1317–1326.

Lessard S, Bigras P, Bonev IA. A new medical parallel robot and its static balancing optimization. J Med Devices 2007;1:272–278.

Levenson J, Pessana F, Gariepy J, Armentano R, Simon A. Gender differences in wall shear-mediated brachial artery vasoconstriction and vasodilation. J Am Coll Cardiol 2001;38:1668–1674.

Nie J, Lu L, Gong X, Nie J, Li Q, Sun M. Determination of lower limb microvasculature by intrafemoral arterial injection using computed tomography-assisted angiography. Aesthetic Plast Surg 2012;36:1376–1381.

Pierrot F, Dombre E, Dégoulange E, Urbain L, Caron P, Boudet S, Gariépy J, Mégnien JL. Hippocrate: A safe robot arm for medical applications with force feedback. Med Image Anal 1999;3:285–300.

Rengier F, Weber TF, Giesel FL, Bockler D, Kauczor HU, von Tengg-Kobligk H. Centerline analysis of aortic CT angiographic examinations: Benefits and limitations. Am J Roentgenol 2009;192:W255–W263.

Roy Cardinal MH, Meunier J, Soulez G, Maurice RL, Therasse E, Cloutier G. Intravascular ultrasound image segmentation: A three-dimensional fast-marching method based on gray level distributions. IEEE Trans Med Imaging 2006;25:590–601.

Schillinger M, Sabeti S, Loewe C, Dick P, Amighi J, Mlekusch W, Schlager O, Cejna M, Lammer J, Minar E. Balloon angioplasty versus implantation of nitinol stents in the superficial femoral artery. N Engl J Med 2006;354:1879–1888.

Watson K, Watson BD, Pater KS. Peripheral arterial disease: A review of disease awareness and management. Am J Geriatr Pharmacother 2006;4:365–379.